Check for updates

Design of Dense Brush Conformation Bearing Gold Nanoparticles as Theranostic Agent for Cancer

Nihan Verimli[1,2] · Ayşegül Demiral[2,3] · Hülya Yılmaz[4] · Mustafa Çulha[4] · S. Sibel Erdem[1,2] (ID)

Abstract

Dense brush conformation–bearing theranostic agents are emerging as drug delivery systems due to their higher ability to escape from reticuloendothelial system uptake which prolongs their in vivo circulation time. With the aim of developing dual therapy agent, 13-nm gold nanoparticles' (AuNPs) surfaces were coated with different amounts of polyethylene glycol (PEG) (SH-PEG-NH$_2$) to obtain dense brush conformation–bearing theranostic agents. Among the 14 different theranostic agent candidates prepared, the one hosting 1819 PEG per particle was selected as the most promising theranostic agent candidate based on structural conformation, stability, size, zeta potential, hemocompatibility, cell inhibition, and cell death pathway towards MCF-7 cell line. To test drug delivery efficiency of the developed PEGylated AuNP and to improve efficacy of the treatment, apoptotic peptide (AP) was covalently conjugated to NH$_2$ terminus of the PEG in various ratios to yield AuNP-AP conjugate. Among the prepared conjugates, the one having 1 nmol of peptide per milliliter of AuNP yielded the most promising results based on the same criteria as employed for PEGylated AuNPs. Besides, incorporation of AP to AuNP returned in superior efficacy of AP since it was possible to achieve 50% cell death with 1000 times less amount of AP alone.

Keywords Apoptosis · Apoptotic peptide · Breast cancer · Drug delivery · Gold nanoparticles · Hemocompatibility · Polyethylene glycol · Theranostic agent

Abbreviations

AP	Apoptotic peptide
BSA	Bovine serum albumin
ATCC	American Type Culture Collection

Nihan Verimli and Ayşegül Demiral contributed equally to this work.

✉ S. Sibel Erdem
serdem@medipol.edu.tr

Extended author information available on the last page of the article

AuNP	Gold nanoparticle
CT	Computed tomography
D	Distance between two PEG attachments
DLS	Dynamic light scattering
DMEM	Dulbecco's modified Eagle's medium
DMSO	Dimethyl sulfoxide
DTNB	5,5′-Dithiobis-(2-nitrobenzoic acid)
EDC	1-Ethyl-3-(3-dimethylaminopropyl) carbodiimide
EPR	Enhanced permeability and retention
FACS	Fluorescence-activated cell sorting
FBS	Fetal bovine serum
FDA	Food and drug administration
IC50	Half maximal inhibitory concentration
LDH	Lactate dehyrdogenase
MTT	(3-(4,5-Dimethylthiazol-2-yl)-2,5-diphenyltetrazolium bromide
MTS	3-(4,5-Dimethylthiazol-2-yl)-5-(3-carboxymethoxyphenyl)-2-(4-sulfophenyl)-2H-tetrazolium
NHS	N-hydroxysuccinimide
PBS	Phosphate-buffered saline
PdI	Polydispersity index
PEG	Polyethylene glycol
PEI	Polyethyleneimine
RES	Reticuloendothelial system
Rf	Flory radius
S	Number of PEG per nanoparticles' surface area
SERS	Surface-enhanced Raman scattering
SH	Sulfhydryl
SPR	Surface plasmon resonance
TEM	Transmission electron microscopy
UV	Ultraviolet
WST	Water-soluble tetrazolium salt

Introduction

Extraordinary surface characteristics, small particle dimensions, availability in different sizes and shapes, relatively easy surface modification, and tunable optical properties make nanoparticles attractive for various biomedical applications [1–4]. Iron oxide nanoparticles, carbon nanotubes, biocompatible polymers, silica and gold nanoparticles are widely used in diagnosis, treatment, and follow-up of different diseases [5]. Among these nanoscale platforms, gold nanoparticles (AuNPs) draw attention due to their unique physical and biological properties, enabling them to be attractive theranostic agents [6].

AuNPs can serve as theranostic even if they are not combined with any drug and/or imaging agent due to their high X-ray attenuation coefficient enabling them to be used as contrast agent for computed tomography (CT) imaging [7]. Besides, stimulation of AuNPs with appropriate wavelength and correspondingly with strong surface plasmon resonance (SPR) causes temperature increase in cells [5]. This is called "photothermal therapy" and it

results with cell damage due to hyperthermia. However, AuNPs are not efficient enough to be used as theranostic agents by themselves. It is crucial to combine these agents with other treatment modalities. Therefore, AuNP surface is usually functionalized with anti-cancer and/ or targeting agents [8].

In order to generate biocompatible theranostic agent, it is essential to coat and functionalize the surface of AuNPs. By coating the surface, (i) stability of AuNP is increased and aggregation of the particles is prevented. (ii) Toxicity is reduced. (iii) Circulation lifetime of the particle is prolonged, and elimination by the reticuloendothelial system (RES) is prevented or slowed down due to decreased interaction with blood proteins. (iv) Modification of the AuNP with drug and/or different agents for targeting and imaging is easily achieved [9]. Dextran, (poly)amino acids, chitosan, polylactic acid, and polyethyleneimine (PEI) are few of the materials that are commonly employed for surface coating of nanoparticles [10–12]. Among these, polyethylene glycol (PEG), approved by FDA (Food and Drug Administration), is the one which takes the most attention. There are currently more than 35 FDA-approved nanoparticles often incorporating PEG, most of which are in preclinical studies for both imaging and therapy. Especially with regard to imaging, PEG is more applicable for surface enhanced Raman scattering (SERS) studies and more preferable than the other biocompatible coating materials such as collagen or bovine serum albumin (BSA) [13, 14].

Due to availability in diverse chain length and different functional groups at the termini, PEG offers flexibility for different chemistries to functionalize nanoparticles' surface to enhance their drug delivery properties [15]. In addition, modifying AuNPs with amphiphilic PEG increases their stability, biocompatibility, and circulation time by decreasing RES uptake. On the other hand, PEG coating increases the affinity for cancer cell membranes and consequently provides more efficient cellular uptake compared to the bare AuNPs [9, 16, 17].

The chain length and/or the amount of PEG on the AuNP surface significantly affect the theranostic agent's behaviour in vitro and in vivo [18]. Depending on the length and the number of the PEG per unit area of nanoparticle, AuNPs obtain three different conformations named as "mushroom," "brush," and "dense brush" [19] (Fig. 1).

Structural conformation is critical for nanoparticles' fate in vivo since stability, and circulation time of the nanoparticles is greatly affected by the attained conformation. Unless nanoparticles have appropriate size and surface coating, they will be easily recognized by the immune system and/or they will be showing increased hemolytic activity. As the density of PEG per unit area increases, the conformation changes from mushroom to dense brush. It is known that nanoparticles having brush conformation are more advantageous for drug delivery purposes due to their increased half-life (~ 19.5 h) in circulation [19].

In the light of aforementioned information, the present study has two specific aims: (i) to investigate the 13-nm citrate stabilized (bare) AuNP's conformation based on the extent of PEG surface coverage to assess the most suitable conformation for development of theranostic agent for the treatment of breast cancer and (ii) to investigate and improve apoptotic peptide's efficacy towards MCF-7 cell line by conjugating it to developed dual therapy offering AuNP-based theranostic drug delivery agent. For this purpose, PEG-coated AuNPs with mushroom, brush, and dense brush conformations were prepared and characterized. To show proof of principle, 9 amino acid bearing apoptotic peptide (AP) was covalently conjugated (Fig. 2) to the AuNP to test drug delivery competence of the newly generated theranostic agent (AuNP-AP). As a first-line requirement for a theranostic agent, dense brush conformation–bearing PEGylated AuNP did not show any toxicity and/or hemolytic activity towards MCF-7 cell line. When AP was immobilized to AuNP surface, the AuNP-AP conjugate did not show any

Fig. 1 Illustration of PEGylated AuNPs with three different conformations depending on the PEG density on the surface. **a** Mushroom. **b** Brush. **c** Dense brush
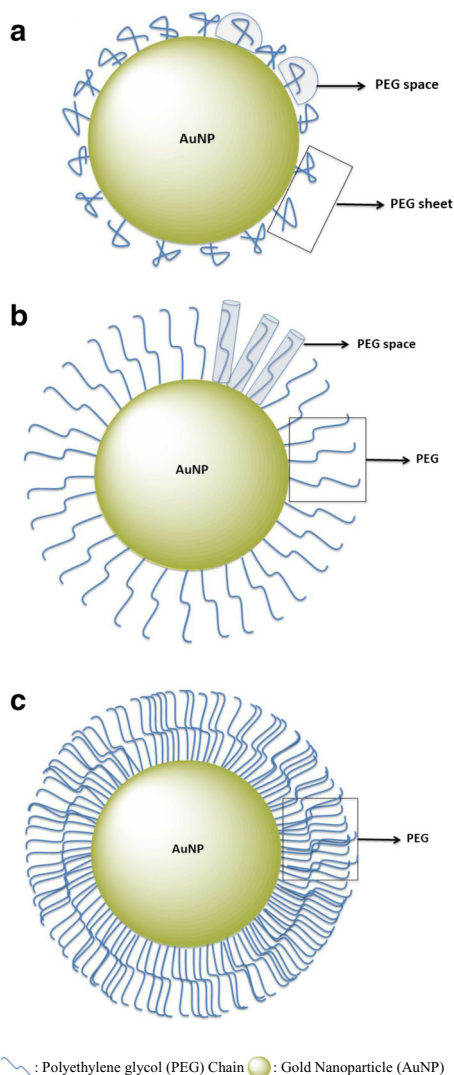

hemolytic activity. Yet, AuNP-AP conjugate showed toxicity towards the selected cell line. In addition, it was possible to achieve higher degree of apoptosis with much less concentration of AP.

Experimental Section

Materials

SH-PEG-NH$_2$ 3500 g/mol and 5,5′-dithiobis-(2-nitrobenzoic acid) (DTNB) were purchased from Sigma-Aldrich. Gold(III) chloride trihydrate (HAuCl$_4$·3H$_2$O) was purchased from Sigma-Aldrich (USA), and trisodium citrate dihydrate (C$_6$H$_5$Na$_3$O$_7$·2H$_2$O) was obtained from

: Apoptotic peptide (AP)
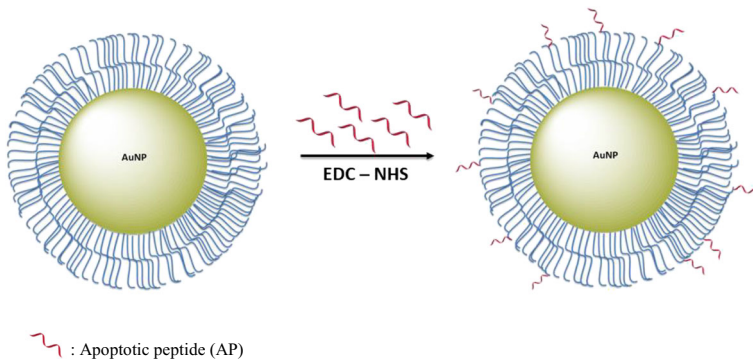
Fig. 2 Immobilization of AP on the surface of the PEGylated AuNP via EDC-NHS coupling and illustration of AuNP-AP conjugate

Merck (Germany). 9-mer AP composed of D amino acids (RLLLRIGRR-NH$_2$) was purchased from GL Biochem. Human breast cancer cells (MCF-7) were purchased from ATCC (American Type Culture Collection). DMEM with high glucose was purchased from Biosera and supplemented with penicillin-streptomycin (10,000 U/mL) purchased from Gibco. FBS was purchased from Biowest. MTT was purchased from ThermoFischer. The wavelength and hydrodynamic size of the spherical AuNPs were measured using UV/Vis spectrophotometer and dynamic light scattering (DLS) (Zetasizer Nano-ZS, Malvern Instruments, Malvern, UK) at a 173° scattering angle with a 4-mW He-Ne laser at room temperature, respectively. The measurements with both UV/Vis spectroscopy and DLS were repeated three times. Spectroscopic measurements were performed using SoftMax® Pro Microplate Reader. AuNPs were centrifuged in ThermoFischer MicroCL 21R Microcentrifuge. Flow cytometric measurements were performed using BioProtect IV with Influx flow cytometry (Baker, BP-504-5). Images of the AuNPs were collected by using Jeol JEM 1400 Transmission Electron Microscope (TEM) at an accelerating voltage of 80 kV.

Cell Cultures

MCF-7 cells were maintained in DMEM medium supplemented with high glucose, penicillin (100 U/mL), streptomycin (100 g/mL), and 10% FBS. The cells were incubated in 5% CO$_2$ incubator at 37 °C and were subcultured twice weekly to maintain subconfluent stocks. In vitro cell studies were performed by seeding 5000 MCF-7 cells per well in a 96-well plate. All experiments were performed in triplicate.

Synthesis and Characterization of 13-nm AuNPs

The spherical 13-nm-sized AuNPs were synthesized by Turkevich method [20]. Briefly, for the synthesis of AuNPs, 40 mg of gold chloride (HAuCl$_4$·3H$_2$O) was first dissolved in 100 mL ddH$_2$O. The solution was stirred and heated until boiling. Then, 10 mL of 38.8 mM trisodium citrate dihydrate solution was rapidly added to the boiling solution. The solution was boiled 15 more minutes after which it was allowed to cool down to room temperature.

The wavelength and hydrodynamic size of the spherical AuNPs were measured using UV/Vis spectrophotometer and DLS, respectively. The measurements with both UV/Vis spectroscopy and DLS were repeated three times. Obtained AuNPs were also examined by TEM [21].

PEGylation of AuNPs

Citrate-stabilized AuNP solution (1 mL, 11 nM) was individually mixed with PEG solutions at 14 different concentrations in a mole ratio ranged from 550:1 to 10,000:1 (PEG:AuNP). In general, AuNP and PEG solutions were mixed and kept at room temperature for 1 h after which the solutions were centrifuged at 14,800 rpm for 30 min at 4 °C and washed twice with same amount of distilled water to remove uncoated PEGs [22]. Supernatants were collected and combined to determine number of PEG chain per particle. Concentrations of AuNPs were spectroscopically determined using Beer-Lambert Law. Hydrodynamic size analysis was performed with DLS. Surface charge of the PEGylated AuNP was measured with Zetasizer Nano Series.

Quantification of Number of PEG per AuNP

Supernatants collected during the PEGylation of AuNPs were treated with Ellman's reagent (5,5′-dithiobis-(2-nitrobenzoic acid)(DTNB) [15]. In general, DTNB reacts with available sulfhydryl (SH) group in the medium and generates 2-nitro-5-thiobenzoic acid in equimolar ratio. By using the 2-nitro-5-thiobenzoic acid's optical density at 412 nm, concentration of PEG in the supernatant was determined. Obtained value was subtracted from the initial PEG amount to determine the PEG amount immobilized to AuNP surface. Ratio of PEG concentration to AuNP concentration yielded the number of PEG per AuNP.

Determination of PEGylated AuNPs' Conformation

Polymer conformation can be determined according to the Flory radius (Rf). Based on the Rf value, we calculated number of PEG chain per AuNP and specified the conformations (mushroom, brush, dense brush) of the AuNPs using the formulas shown below (Table 1) [19].

As an example, calculation of Rf value for 550:1 (PEG:AuNP) sample was detailed below. The area of 13-nm spherical AuNP was calculated as 530.66 cm^2 (Eq. 1), and the S value, which represents the number of the PEG per unit area, of 550:1 (PEG:AuNP) sample was determined as 0.09 by dividing 46 to 530.66 (Eq. 2). D value, representing the distance between two PEG chains, was found by employing Eq. 3. In the last step, Flory radius (Rf) was determined using the length of one monomer (α) and the number of monomers per PEG chain

Table 1 Formula list for determination of polymer conformation

Equation number	Equation
Eq. 1	Area $= 4\pi r^2$
Eq. 2	$S =$ Number of PEG/Area
Eq. 3	$D = 2(1/S\pi) \cdot (0.5)$
Eq. 4	$Rf = \alpha N^{3/5}$

S: number of PEG per nanoparticles' surface area; D: the distance between two PEG attachments; Rf: flory radius; $Rf/D > 1$: brush conformation; $Rf/D \lesssim 1$: mushroom conformation

(N) (Eq. 4). For PEG3500, α is 0.35 nm and N is 80; therefore, Rf is 4.85 nm. Finally, the Rf/D value gives the conformation of the PEGylated AuNPs.

Conjugation of PEGylated AuNPs with AP

PEGylated AuNP solution (1 mL, 11 nM) was individually mixed with 9-mer AP solutions in the presence of 1-ethyl-3-(3-dimethylaminopropyl)carbodiimide (EDC) and N-hydroxysuccinimide (NHS) at 3 different concentrations in molar ratios of 5:1, 10:1, and 20:1 (PEG:AP). In general, 2500:1 (PEG:AuNP) AuNPs, AP, EDC, and NHS were mixed in 1:7.5:1.5 eq (AP:EDC:NHS) ratio in 30% DMSO in water. pH of the solution was adjusted to 8–9 using Triethylene amine and left for overnight incubation at 37 °C [23]. The solution was centrifuged at 14,800 rpm for 30 min at 4 °C and washed twice with same amount of water. Conjugates are also stable in 30% DMSO solution and cell culture medium (DMEM). Concentration of the conjugate was spectroscopically determined using Beer-Lambert Law. Hydrodynamic size analysis was performed with DLS. Surface charge of the conjugate was measured with Zetasizer Nano Series. AP concentration was calculated based on the PEG:AP mole ratio. For instance, for the 5:1 conjugate, there are 20 nmol PEG and 4 nmol AP yielding roughly 400 AP per PEGylated AuNP.

Cytotoxicity Assay

To evaluate PEGylated AuNPs' toxicity towards the selected cell line, MTT (3-(4,5-di methyl thiazol-2-yl)-2,5-diphenyltetrazolium bromide) assay was carried out. MTT assay is widely used in the literature as a cell viability assay since it is inexpensive and compatible with the selected nanoparticles [24, 25]. As a general procedure, cells were seeded into 96-well plate as 5000 cells per well and let to adhere surface for 36–48 h. Cells were separately incubated with bare AuNPs, PEGylated AuNPs having brush and dense brush conformations, AuNP-AP conjugate (in the range of 0.25–4 nM AuNP; 88–700 nM AP with 6 different concentrations), and AP alone (60–480 μM) for 24 h. Five microliters of MTT solution (5 mg/mL in phosphate-buffered saline (PBS)) was added to each well and allowed to incubate for another 3 h to yield formazan crystals. Following the removal of MTT solution, dimethyl sulfoxide (DMSO) (200 μL) was added to the each well and the plate was left in shaker for 30 min. Optical density at 570 nm measured by a plate reader. The relative cell viability (%) was expressed as a percentage relative to the untreated control cells (100% viable) and the cells treated with detergent Triton X (0% viable).

Determination of Hemolytic Activity

For the purpose of determination of hemolytic activity of bare AuNPs, PEGylated AuNPs, AuNP-AP conjugate, and AP alone, the hemolysis assay was carried out by modifying the method described by Chen et al. [26]. Briefly, a sample of whole blood centrifuged at 3500 rpm for 5 min and the plasma was replaced with PBS (pH 7.4) solution. This process was repeated three times, and the collected erythrocytes were diluted with PBS in 1:10 volume ratio. For every sample that would be tested, 1 mL of diluted erythrocyte solution was taken to an eppendorf tube and the required volume of sample was added to the erythrocyte solution to achieve desired concentration and incubated at 37 °C for 1 h. Following the incubation,

eppendorf tubes were centrifuged at 14,800 rpm for 30 min to remove erythrocytes from the solution. Optical density of the supernatant was measured at 541 nm wavelength.

One percent of Triton X-100 was used as positive control, and hemolysis of the materials was calculated by following equation:

$$Hemolysis\% = (Test\ well - Negative\ Control)/(Positive\ Control - Negative\ Control) \times 100$$

### Determination of Cell Death Pathway

A total of 2×10^5 cells were plated in 35-mm petri dish and allowed to adhere for 24 h. Following the confirmation of cell adhesion with light microscope, the cells were incubated individually with PEGylated AuNPs, AuNP-AP conjugate, and AP alone at their determined IC50 concentrations. eBioscience Annexin V-FITC Apoptosis Detection Kit was used to determine cell death mechanism for each group individually following manufacturer's instructions. Briefly, the fixed cells were incubated with Annexin V FITC for 10 min after which they were washed with 1× binding buffer. The fixed cell was taken into PBS and incubated with PI for 3 min. Following the removal of excess of PI with PBS twice, images were taken employing the following excitation and emission wavelengths: Annexin V FITC (ex/em 494 nm/518 nm) and PI (ex/em 358 nm/461 nm). Nine microscopic fields were scanned at a magnification of 20 Å~ for each petri dish. ImageJ software (National Institute of Health) was used for image analysis. Apoptosis/necrosis ratio was calculated based on the cell numbers in each group.

Results and Discussion

The spherical AuNPs were synthesized by employing the well-known Turkevich method. Characterization of bare AuNPs was achieved via spectroscopic methods, DLS and TEM (Fig. 3), as well as zeta-potential measurements to find out their concentrations, hydrodynamic sizes, and surface charges, respectively. As reported in literature, λmax of 13-nm AuNPs was measured at 520 nm (supplementary material). Initially, using Beer-Lambert Law at λmax(520 nm), concentration of the bare AuNPs was determined as 11 nM. The mean hydrodynamic size (Z-average) of the prepared spherical AuNPs was estimated at 13 ± 2 nm with polydispersity index (PdI) of 0.187 from DLS measurement, and the surface charge was detected as -32.3 mV (supplementary material). Based on the analyses, AuNPs exhibited favorable colloidal properties.

In order to obtain stable PEGylated AuNPs having mushroom, brush, and dense brush conformations, AuNPs were treated with different amounts of commercially available PEG (SH-PEG-NH$_2$, 3500 g/mol). While keeping the AuNP concentration constant, mole ratios of PEG were ranged from 550 to 10,000 as shown in Table 3. In order to precisely assess the AuNP's conformation, it is critical to know the number of PEG on a single AuNP. Therefore, for each prepared AuNP, PEG number per AuNP was determined by employing Ellman's method [14]. As the ratio of PEG over AuNP increased, number of PEG immobilized on the AuNP surface increased as well (Fig. 4). Based on the calculations, while 550:1 (PEG:AuNP) yielded 46 PEG per particle, 2500:1 (PEG:AuNP) gave 1819 PEG per particle. Beyond 2500:1 (PEG:AuNP) ratio, increasement of the ratio did not significantly change the immobilized
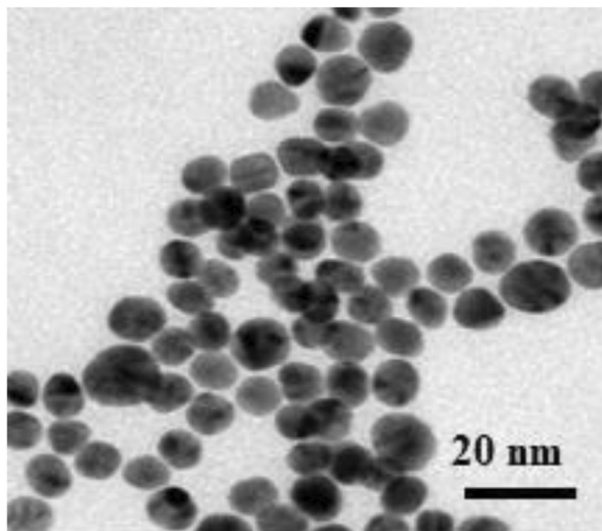
Fig. 3 TEM image of bare 13-nm AuNPs

PEG number on the AuNP surface. For example, 10,000:1 (PEG:AuNP) gave 1862 PEG per AuNP (Fig. 4).

PEGylation study results suggested that stable AuNPs were obtained only when PEG was used in a ratio greater than 1000:1 (PEG:AuNP). Below 1000:1 ratio, AuNP precipitated out within 1 to 24 h time period. Due to SH group's high affinity towards Au, AuNPs' surface was easily modified with SH-PEG-NH$_2$, exposing NH$_2$ terminus on the PEG corona. As three carboxylic acid bearing citrate was replaced with PEG, AuNP surface charge was changed from − 32.3 to 6.35 mV (Table 2) and the size of AuNPs was increased from 13.24 nm to up to 30.64 nm depending on the degree of PEGylation (Table 2). Increase of the PEG:AuNP ratio did not significantly affect neither size nor zeta potential of the agent due to saturation of AuNP surface and inability of addition of more PEG to the surface beyond
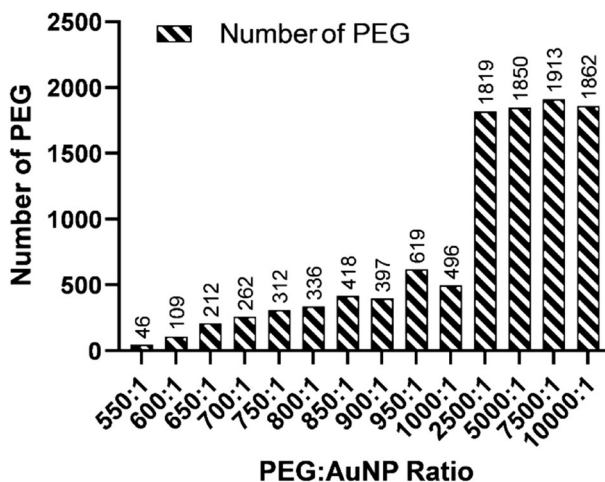
Fig. 4 Number of immobilized PEG per AuNP for different PEG:AuNP ratios

2500:1(PEG:AuNP) ratio. For instance, while 1000:1 (PEG:AuNP) has 27.91 nm size and 6.25 mV zeta potential, 10,000:1(PEG:AuNP) has 27.84 nm size and 5.24 mV zeta potential.

All AuNPs' conformations were determined according to the calculations detailed in methods section [27]. It was not possible to obtain mushroom conformation bearing theranostic agent by employing 13-nm AuNPs and PEG3500 since following PEGylation, mushroom conformation AuNPs were immediately aggregated. In order to develop mushroom conformation bearing AuNPs, either shorter PEG having smaller Rf value or AuNPs with larger diameter has to be combined. Based on the theoretical calculations, when PEG:AuNP ratio was between 550:1 and 650:1, AuNPs obtained brush conformation yielding 46–250 PEG per particle (Table 3). Brush conformation–bearing AuNPs could not be fully characterized since they were unstable and precipitated out in a matter of hours clearly indicating that PEG density on the surface greatly affects the stability of the particles. As the PEG:AuNP ratio increased to equal or above 700:1, AuNPs obtained dense brush conformation yielding 250–1900 PEG per particle (Table 3). Even though we were able to obtain more stable AuNPs compared to mushroom and/or brush conformation, stability was still not in the acceptable range for a drug delivery agent. For instance, AuNPs having 700:1–1000:1 (PEG:AuNP) ratio were not as stable as the ones having greater than 1000:1 (PEG:AuNP) ratio AuNPs. Stability of the AuNPs was precisely proportional to the PEG:AuNP ratio. Even 50 PEG unit difference per AuNP has an impact on the overall stability of the particle. For instance, even though 700:1 and 2500:1 fall into the same category (dense brush), stability of 2500:1 is much greater than 700:1 since denser PEG coating provides better shielding of the nanoparticle's interaction from the environment [28]. We further investigated the prepared AuNPs' stability by resuspending them in various solutions such as 100% DMEM, 100% distilled water, DMSO:DMEM (1:99 v/v), and DMSO:water (30:70 v/v) solutions. AuNPs having greater than 1000:1 (PEG:AuNP) ratio were stable without any aggregation and maintained their characteristics both at room temperature and 37 °C. In addition, all AuNPs can be stored at 4 °C for at least 3 months.

In order to evaluate PEGylated AuNPs' toxicity towards the selected cell line, MTT assay was used. There are other cytotoxicity assays such as (3-(4,5-dimethylthiazol-2-yl)-5-(3-carboxymethoxyphenyl)-2-(4-sulfophenyl)-2H-tetrazolium) (MTS) assay, lactate dehyrdogenase (LDH) assay, netural red cytotoxicty assay, water-soluble tetrazolium salt (WST) assay, and real-time xCELLigence impedance assay, which are compatible with gold nanoparticles [29, 30] Among these, MTT assay was employed for this study. The cells were incubated with bare and PEGylated AuNPs up to 48 h in different concentrations ranging from 0.25 to 4 nM AuNPs. The results indicated that the bare AuNPs were toxic towards MCF-7 cell line even as low as 0.25 nM concentration following both 48 h and 24 h incubation time (24 h data is not shown). For instance, after 48 h incubation period, only 60% cell viability was

Table 2 Size and zeta potential of PEGylated AuNPs

| Group	Size (d nm)	Zeta potential (mV)
Citrate stabilized AuNP	13.24	− 32.3
1000:1 (PEG:AuNP)	27.91	6.25
2500:1 (PEG:AuNP)	30.64	6.28
5000:1 (PEG:AuNP)	28.89	5.98
7500:1 (PEG:AuNP)	29.38	6.35
10,000:1 (PEG:AuNP)	27.84	5.24

Table 3 Determination of the conformation of PEGylated AuNPs

Group (PEG:AuNP)	Area	No. of PEG	S	A	D	Rf	Rf/D	Conformation
550:1	530.66	46	0.09	11.1	3.76	4.85	1.29	Brush
600:1	530.66	109	0.21	4.76	2.46	4.85	1.97	Brush
650:1	530.66	212	0.40	2.5	1.78	4.85	2.72	Brush
700:1	530.66	262	0.50	2	1.60	4.85	3.03	Dense brush
750:1	530.66	312	0.59	1.69	1.47	4.85	3.29	Dense brush
800:1	530.66	336	0.63	1.59	1.42	4.85	3.42	Dense brush
850:1	530.66	418	0.79	1.27	1.27	4.85	3.82	Dense brush
900:1	530.66	397	0.75	1.33	1.30	4.85	3.73	Dense brush
950:1	530.66	619	1.12	0.89	1.06	4.85	4.58	Dense brush
1000:1	530.66	496	0.93	1.08	1.17	4.85	4.15	Dense brush
2500:1	530.66	1819	3.43	0.29	0.61	4.85	7.95	Dense brush
5000:1	530.66	1852	3.49	0.29	0.61	4.85	7.95	Dense brush
7500:1	530.66	1917	3.61	0.28	0.60	4.85	8.08	Dense brush
10,000:1	530.66	1835	3.46	0.29	0.61	4.85	7.95	Dense brush

achieved with 3 nM bare AuNP (Fig. 5a). Like in the case of stability of the AuNPs, as the PEG:AuNP ratio increased, it was possible to achieve higher degree of cell viability. For instance, cell viabilities of 550:1 (PEG:AuNP), 900:1 (PEG:AuNP) and 2500:1 (PEG:AuNP) were obtained as 82%, 86%, and 93%, respectively data not shown. As the concentration of AuNP decreased to 2 nM, it was possible to reach 99% cell viability with 2500:1 (PEG:AuNP) ratio in the same incubation period (Fig. 5b and 5c). Size, zeta potential, number of PEG per particle, particle's conformation, stability, and viability results suggested that among the prepared AuNPs, 2500:1 (PEG:AuNP) is the most suitable one for the desired drug delivery application. In addition, above this ratio, neither the size, zeta potential, and stability nor number of PEG per AuNP dramatically changed. Therefore, the rest of the study was carried out by using AuNPs having 2500:1 (PEG:AuNP) mole ratio.

Hemocompatibility is one of the most important parameters for any agent and/or drug that is aimed to be used in vivo systems [31]. In order to confirm that the selected AuNPs are hemocompatible, hemolysis assay was performed for bare AuNPs and 2500:1 (PEG:AuNP) AuNPs individually. Following the isolation of healthy red blood cells from volunteer's freshly taken blood, erythrocytes were incubated with the selected samples with AuNP concentration ranging from 0.5 to 4 nM. Hemolysis percentages of the samples were determined employing optical density at 541 nm, which belongs to hemoglobin's absorbance. The hemolysis percentages of the bare AuNPs and 2500:1 (PEG:AuNP) AuNPs were less than 2% even at the highest selected concentration of the particles. These results clearly indicated that neither bare AuNPs nor 2500:1 (PEG:AuNP) AuNPs show any visible hemolytic activity at the deliberated concentration range, which makes the AuNP favorable candidate as a drug delivery agent.

Following the synthesis and characterization of 2500:1(PEG:AuNP) AuNPs, the study was extended to show proof of principle of the AuNPs as theranostic agent. For this purpose, nine amino acids bearing AP was immobilized on the surface of the AuNP. Previously, it was shown that the AP was tested towards macrophages, erythrocytes, as well as fibroblasts and did not show any cytotoxicity [32]. In addition, anti-cancer activity of the AP has also been shown in various adenocarcinoma cell lines such as the kidney, lung, and glioblastoma [33]. In all cases, the AP showed toxicity towards to the aforementioned cancer cell lines with IC50 value in a range from 50 to 640 μM. These IC50 values are high to be considered the AP as an
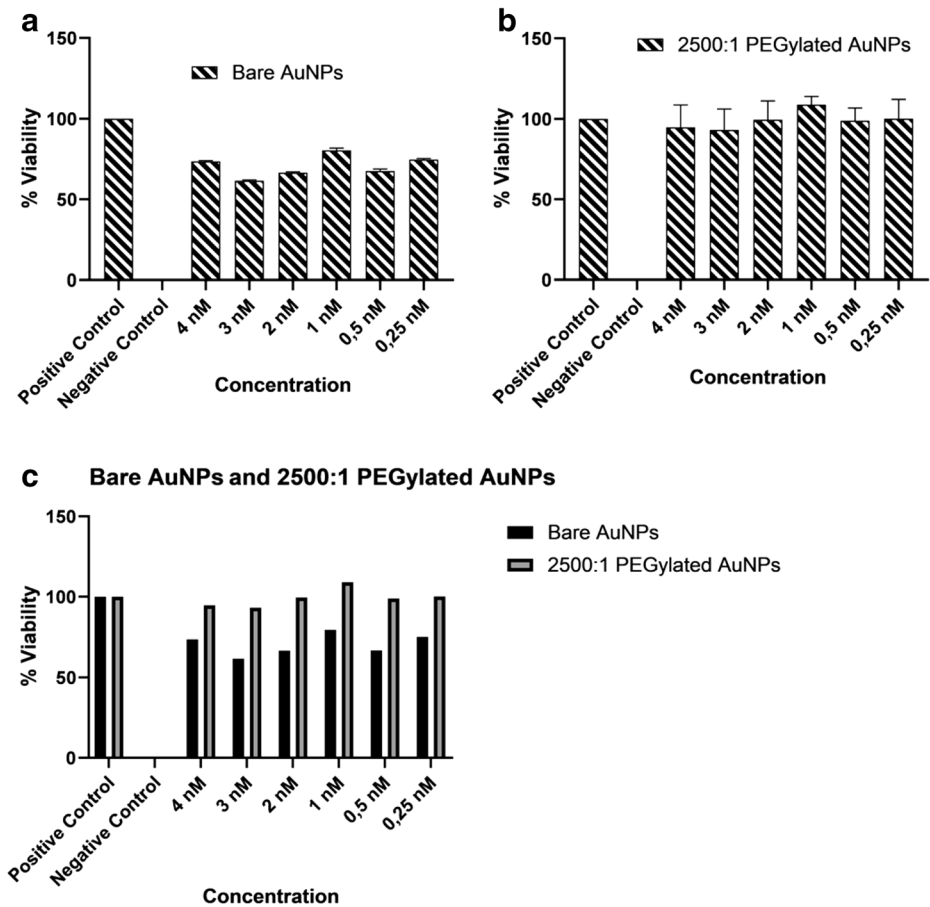
Fig. 5 Cytotoxicity of bare and PEGylated AuNPs towards MCF-7 cell line following 48 h incubation. **a** Bare AuNPs. **b** 2500:1 (PEG:AuNP) AuNPs. **c** Bare and 2500:1 (PEG: AuNP) PEGylated AuNPs

anti-cancer drug candidate. Therefore, it is crucial either to generate combination therapy with the AP and/or improve its toxicity via combining it with drug delivery agents. Our group has conducted a study with the identical 9-mer AP to improve its anti-cancer activity towards ovarian cancer [33]. We successfully demonstrated the synergism between the AP and FDA-approved photodynamic therapy drug called Verteporfin in a sequence-dependent combination therapy towards ovarian cancer cell line. To the best of our knowledge, there is no study in the literature combining the 9-mer AP with any drug delivery vehicle to enhance its cytotoxicity via lowering the required dose and/or reduce the any possible side effects in vivo. Therefore, in order to show 2500:1 (PEG:AuNP) AuNP drug delivery feature and to develop dual therapy offering dense brush conformation–bearing AuNPs, the C-terminus of the AP was conjugated to NH_2 terminus of the PEG on the AuNP surface via EDC-NHS chemistry. Based on the Ellman's method, there are roughly 1819 PEG per AuNP which is corresponding to 20 nmol PEG in 1 mL of AuNP solution. Briefly, 2500:1 (PEG:AuNP) AuNPs were mixed with the AP in 5:1, 10:1, and 20:1 (PEG:AP) mole ratio. Following overnight incubation, AuNPs were centrifuged and resuspended in water. AP amount for each conjugate was estimated based on the mole ratio of PEG over AP. Mole number of AP per 2500:1 (PEG:AuNP) AuNP was

calculated as 4, 2, and 1 nmol for 5:1, 10:1, and 20:1, respectively. These numbers were translated to number of AP per 2500:1 (PEG:AuNP) AuNP as 400, 200, and 100 for 5:1, 10:1, and 20:1, respectively (Table 4). Size and zeta potential measurements were performed for each conjugate. The results showed that the ratio of PEG:AP was inversely proportional to the size of the AuNP-AP conjugate, indicating higher to lower degree of aggregation of the nanoparticles (Table 4) (supplementary material). We believe that, since AP is mostly composed of nonpolar amino acids, increased amount of AP on AuNP causes aggregation of the particles.

Following the characterization, MCF-7 cells were incubated with each conjugate separately for 24 h using ranges of AuNP concentration from 0.5 to 4 nM. Cell viability assay results were also in agreement with the aggregation phenomenon. Despite the fact that 5:1 and 10:1 carried more AP, they caused less toxicity towards MCF-7 cell line. For instance, 69% and 63% cell viabilities were obtained with 2 nM AuNP containing 5:1 and 10:1 (PEG:AP) conjugates, respectively. We believe that the aggregation of the AuNP-AP conjugates interferes with the interactions of the nanoparticles with the cell surface and reduces cell uptake and leads further aggregation in subcellular level [34]. Consequently, all these can be considered as precipitating factors to cause less toxicity towards the selected cell line. For instance, even though amount of AP on the 20:1 (PEG:AP) AuNP-AP conjugate was 4 times less than the 5:1(PEG:AP) conjugate's, it was possible to achieve 50% cell death with much lower concentration of AP (4 vs 1 nmol). A total of 10:1 and 5:1(PEG:AP) AuNP-AP conjugates showed the similar pattern as well. While 5:1 was hosting more number of AP, 10:1 conjugate yielded higher degree of cell death at equimolar AuNP concentration. While 2 nM AuNP and 704 nM (1 nmol) AP containing 10:1 (PEG:AP) conjugate caused 37% cell death, 2 nM AuNP and 1408 nM (2 nmol) AP containing 5:1 (PEG:AP) conjugate leaded 31% cell death (Fig. 6a, b). In the case of 20:1 (PEG:AP), 50% cell viability (IC50) was achieved with 2 nM AuNP and 352 nM (0.5 nmol) AP-containing conjugate (Fig. 6c, d). Following examination of the conjugates, we also carried out MTT assay for the AP, which is the second component of the desired drug delivery agent. As mentioned before, AP showed toxicity towards to the MCF-7 cells above 60 μM concentration (Fig. 6e). Based on the cell viability assay results, IC50 value of AP was determined as 316 μM (Fig. 6f), which is high to consider the AP as an anti-cancer drug candidate.

Dose reduction of the AP is advantageous to achieve equal or better efficacy with much lower drug concentration. Among the prepared conjugates, due to its higher stability, lower degree of aggregation, and higher cell death ratio, 20:1 (PEG:AP) AuNP-AP conjugate was chosen for further evaluations. In addition, since AP is immobilized to AuNP-PEG surface via stable amide bonds, loss of AP from the particle surface was not detected via zeta potential and DLS measurement within 3 months (data not shown).

Table 4 Size and zeta potential of citrate-stabilized, PEG-functionalized, and AP-conjugated gold nanoparticles

Group	Size (d nm)	Zeta potential (mV)
Bare AuNP	13.24	− 32.30
2500:1 PEGylated AuNP	30.64	6.28
5:1 (PEG:AP) conjugate	204.6	2.34
10:1(PEG:AP) conjugate	113.3	4.30
20:1 (PEG:AP) conjugate	53.6	1.33
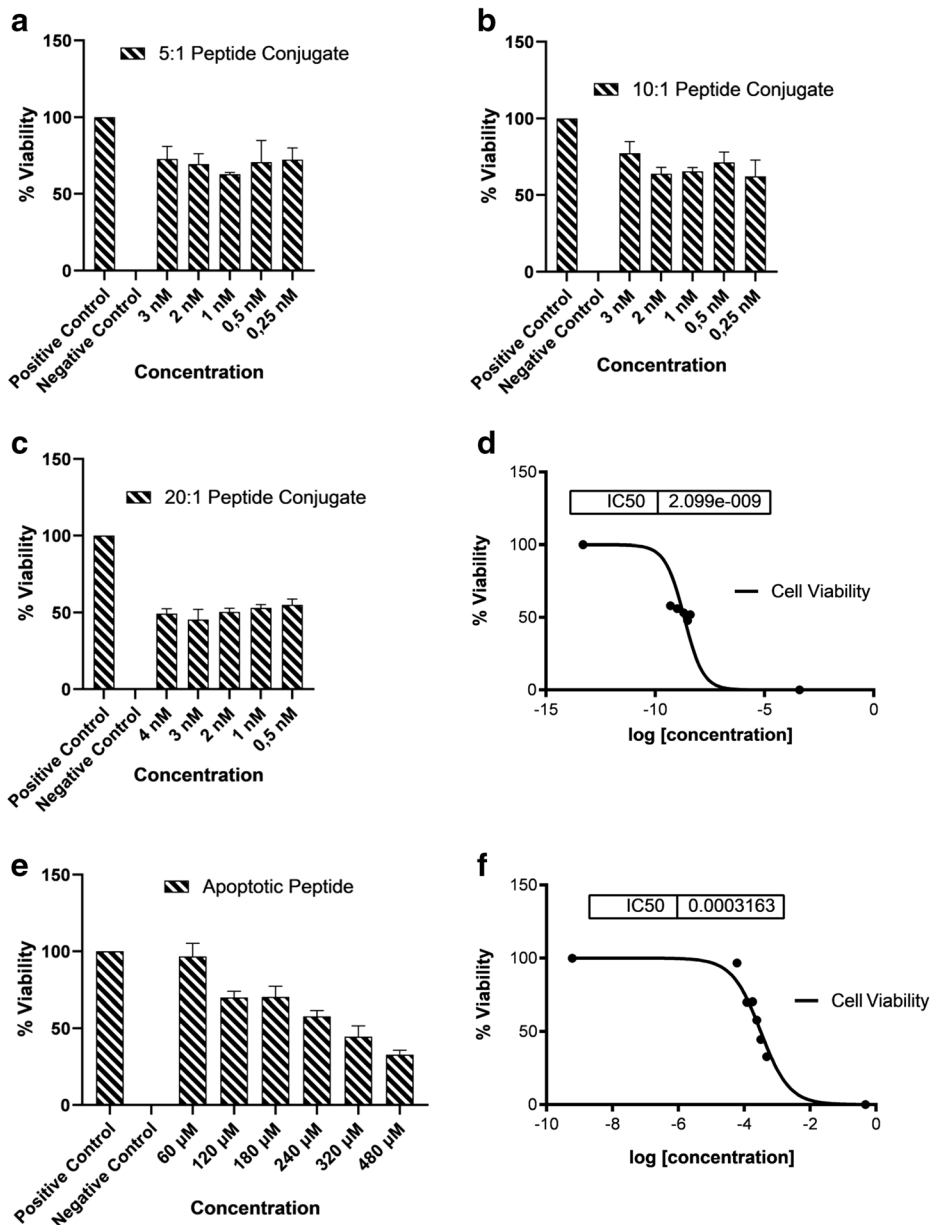
Fig. 6 Cytotoxicity of AuNP-AP conjugates and AP only towards MCF-7 cell line following 24 h incubation. **a** 5:1 (PEG:AP) conjugate. **b** 10:1 (PEG:AP) conjugate. **c** 20:1 (PEG:AP) conjugate. **e** AP alone. IC50 values of **d** 20:1 (PEG:AP) conjugate and **f** AP alone

Hemocompatibility studies for the AP (50 nM-320 μM) and AuNP-AP (0.5–4 nM AuNP; 0.125–1 nmol; 88–704 nM AP) were conducted separately. Even at the highest concentration for the each agent, hemolysis rate did not exceed above 2%. These results clearly revealed that neither AP nor the AuNP-AP conjugate caused hemolysis at the selected concentration ranges (Fig. 7).

In order to determine the cell death pathway, fluorescence-activated cell sorting (FACS) analyses were performed for 2500:1 (PEG:AuNP) AuNPs, 20:1 (PEG:AP) conjugate, and AP only. Briefly, MCF-7 cells were separately incubated with 2 nM 2500:1 (PEG:AuNP) AuNPs, 2 nM AuNP and 352 nM AP bearing 20:1 (PEG:AP) conjugate and 316 μM AP alone for 24 h. Following the incubation, the cells were fixed, labeled with Annexin and PI, and scanned to determine apoptosis over necrosis ratio for each group. As a control experiment, the cells were fixed and labeled with the same dyes without any treatment. The results showed that in the control group, 80.81% of the cells were at the living, 8.19% of them were at the necrotic, and 9.49% were at the early apoptotic stages (Fig. 8a). When the cells were treated with 2 nM 2500:1 (PEG:AuNP) AuNPs, 85.80% of the cells were alive while 4.54% was at the necrotic and only 8.40% was at the early apoptotic stages (Fig. 8b). There were negligible amount of cells at the late apoptotic stage for this group. When the cells were treated with 316 μM of apoptotic peptide, only 50.05% of the MCF-7 cells were alive. A total of 19.67% of the cells were at necrotic, 8.12% of the cells were at the late apoptotic, and 19.14% of the cells were at the early apoptotic stage overlapping with the AP's cell death mechanism (Fig. 8c) [32]. As a result of 2 nM AuNP and 352 nM AP bearing 20:1 (PEG:AuNP) conjugate treatment, 54.39% of the MCF-7 cells were alive (Fig. 8d). While 35.77% of the cells were at the early apoptotic stage, only 1.71% of them were at the late apoptotic and 5.19% of them was at the necrotic stage (Fig. 8d).

All samples roughly had same amount of necrosis rate as the control experiment outlining necrosis as the cell death mechanism for the investigated groups. On the other hand, predominant cell death pathway was apoptosis both for AuNP-AP and AP which is in agreement with the cell death mechanism of AP as well [32]. When we compared the live and apoptotic cell ratio, the results clearly indicated that following 2500:1 (PEG:AuNP) AuNPs treatment, large majority of the cells were alive, while the equimolar AuNP and 352 nM AP containing AuNP-AP treatment leaded apoptosis in 35.77% of the cells. On the other hand, when the cells were treated with only AP at 316 μM, which is the IC50 value of AP, 19.67% of the cells were at the early apoptotic stage. This number was increased almost twice as much to 35.77% with roughly 1000 times less AP hosting conjugate (352 nM). All these obtained data are in agreement with the cell viability results as well. We speculate that the peptide delivery to the cell is much more efficient when it was carried with an appropriate drug delivery agent, AuNP. Therefore, by treating the cells with 1000 times less amount of AP, 50% of cell death was achieved. It is known that AuNPs enhance cellular uptake and consequently increases efficacy of the treatment [35–37] which is overlapping with our results.

Conclusion

Results of this study showed that depending on the number of PEG unit, the length of the PEG chain, and the size of the AuNP, it was possible to achieve brush and dense brush conformation–bearing AuNPs by employing 13-nm AuNPs and PEG3500 at different mole ratios. The number of immobilized PEG was proportional to the stability of the AuNP, and above 1000:1 (PEG:AuNP) ratio, stability of the AuNPs tremendously increased. Among the 14 different theranostic agent candidates, conformation of 2500:1 (PEG:AuNP) was determined as "dense brush" and number of PEG per AuNP was estimated at 1819. A total of
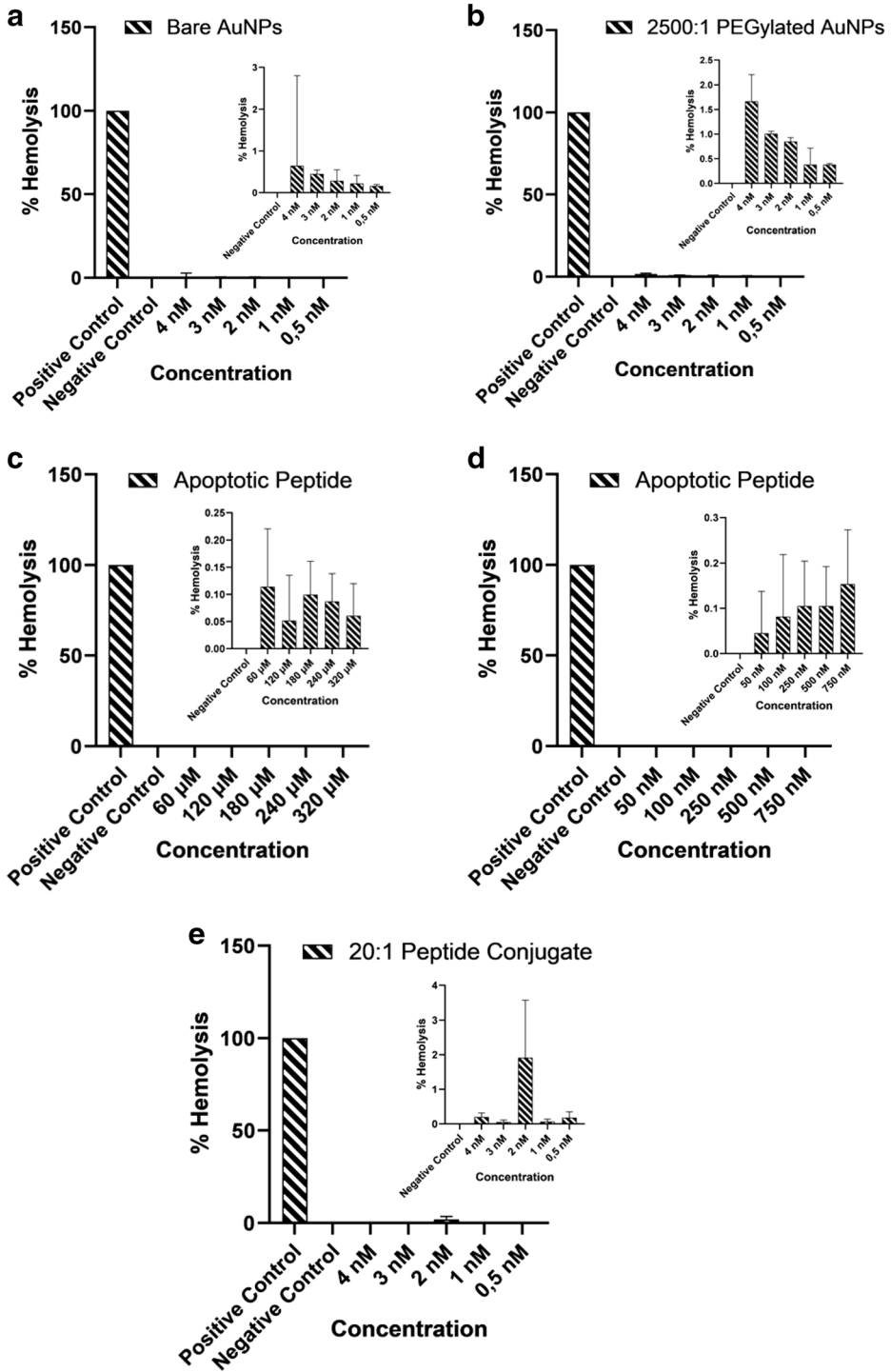
◀ **Fig. 7** Mean hemolytic assay results. Erythrocytes exposed to **a** bare AuNPs, **b** PEGylated AuNPs, **c** higher, and, **d** lower concentrations of apoptotic peptide are compared with those exposed to PBS solution (negative control) and Tween 20 (positive control) **e** 20:1AuNP-AP conjugate

2500:1 (PEG:AuNP) AuNP was selected as the promising theranostic agent since it did not show any toxicity towards MCF-7 cell line and did not show any significant hemolytic activity. Besides, their long-term stability in various aqueous solutions and less than 100 nm size made 2500:1 (PEG:AuNP) AuNP attractive candidate as theranostic agent [38].

One of the aims of the study was successfully achieved by incorporating AP to the AuNP surface. Among three different AuNP-AP conjugates, due to its hemocompatibility and high stability, 20:1 (PEG:AP) AuNP was chosen as the most promising one. Well overlapping with the purpose of this study, this conjugate has the least amount of AP but yielded the highest cell death ratio in comparison to the two other prepared AuNP-AP conjugates. In addition, our results showed that when the cells were treated with AP alone, it was required to use 1000 times more AP compared to the AP amount on the 20:1 (PEG:AP) AuNP conjugate towards MCF-7 cell line.

With the accomplishment of the presented study, we not only proved the drug delivery feature of 2500:1 (PEG:AuNP) but also were able to show that much less amount of AP could be used to induce apoptosis in MCF-7 cell line. Achieved dose reduction is critical for any drug candidate to improve its efficacy and reduce its side effects. In conclusion, AuNP-based, imaging, and dual therapy–offering theranostic agent was developed. This agent can be used for diagnosis and treatment of cancer and any other diseases of interest.

As future work, functionalization of these theranostic agents with a targeting moiety would enhance the efficacy of these developed systems and provide better diagnosis and treatment possibilities. As continuation of this study, we will be further investigating the developed theranostic agent in vitro and in vivo systems.
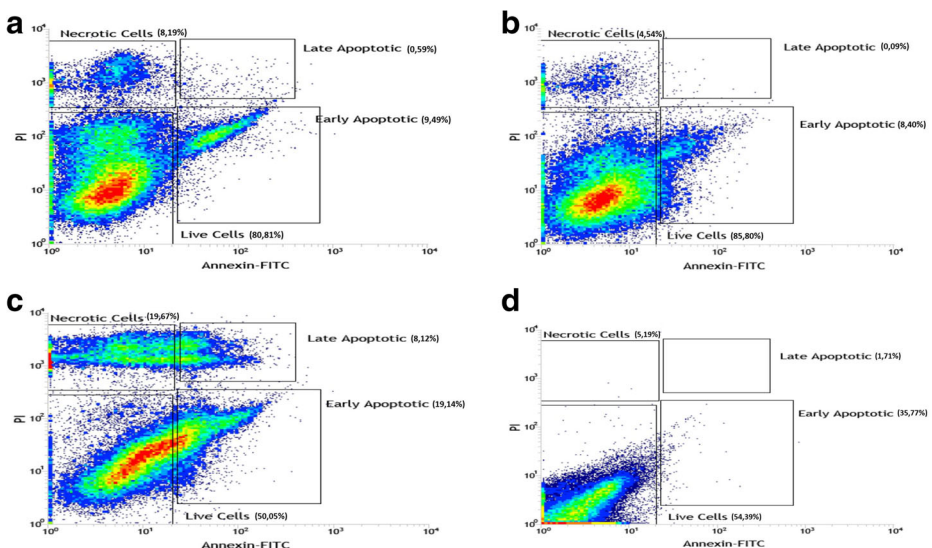
Fig. 8 FACS analysis of Annexin V/propidium iodide. **a** Control. **b** 2500:1 (PEG:AuNP) AuNPs (2 nM). **c** AP (316 μM). **d** 20:1 (PEG:AP) conjugate (2 nM AuNP and 352 nM AP) for 24 h

Compliance with Ethical Standards

Conflict of Interest The authors declare that they have no conflict of interest.

Ethical Issues Istanbul Medipol University Non-Invasive Clinical Research Ethical Committee with issue number 10840098-604.01.01.-E.16355.

References

1. Cho, K., Wang, X., Nie, S., Chen, Z., & Shin, D. M. (2008). Therapeutic nanoparticles for drug delivery in cancer. *Clinical Cancer Research, 14*(5), 1310–1316. https://doi.org/10.1158/1078-0432.CCR-07-1441.
2. Conde, J., Dias, J. T., Grazừ, V., Moros, M., Baptista, P. V., & de la Fuente, J. M. (2014). Revisiting 30 years of biofunctionalization and surface chemistry of inorganic nanoparticles for nanomedicine. Frontiers in Chemistry, 2(July), 1–27. https://doi.org/10.3389/fchem.2014.00048.
3. Dreaden, E. C., Austin, L. A., Mackey, M. A., & El-Sayed, M. A. (2012). Size matters: gold nanoparticles in targeted cancer drug delivery. *Therapeutic Delivery, 3*(4), 457–478. https://doi.org/10.4155/tde.12.21.
4. Ma, A., & Czechowska, E. (2018). Immobilization of recombinant human catalase on gold and silver nanoparticles. *Applied Biochemistry and Biotechnology, 185*(3), 717–735. https://doi.org/10.1007/s12010-017-2682-2.
5. Fernandez-fernandez, A., Manchanda, R., & Mcgoron, A. J. (2011). Theranostic applications of nanomaterials in cancer: drug delivery, image-guided therapy, and multifunctional platforms. *Applied Biochemistry and Biotechnology, 165*(7–8), 1628–1651. https://doi.org/10.1007/s12010-011-9383-z.
6. Singh, P., Pandit, S., Mokkapati, V. R. S. S., Garg, A., Ravikumar, V., & Mijakovic, I. (2018). Gold nanoparticles in diagnostics and therapeutics for human cancer. *International Journal of Molecular Sciences, 19*(7). https://doi.org/10.3390/ijms19071979.
7. Cormode, D. P., & Fayad, Z. A. (2011). Nanoparticle contrast agents for CT: their potential and the challenges that lie ahead, 3, 263–266.
8. Chatterjee, D. K., Diagaradjane, P., & Krishnan, S. (2011). Nanoparticle-mediated hyperthermia in cancer therapy. *Therapeutic Delivery, 2*(8), 1001–1014. https://doi.org/10.4155/tde.11.72.
9. Pissuwan, D., Niidome, T., & Cortie, M. B. (2011). The forthcoming applications of gold nanoparticles in drug and gene delivery systems. *Journal of Controlled Release, 149*(1), 65–71. https://doi.org/10.1016/j.jconrel.2009.12.006.
10. Jokerst, J. V., Lobovkina, T., Zare, R. N., & Gambhir, S. S. (2011). Nanoparticle PEGylation for imaging and therapy. *Nanomedicine, 6*(4), 715–728. https://doi.org/10.2217/nnm.11.19.
11. Gupta, A. K., & Gupta, M. (2005). Synthesis and surface engineering of iron oxide nanoparticles for biomedical applications. *Biomaterials, 26*(18), 3995–4021. https://doi.org/10.1016/j.biomaterials.2004.10.012.
12. Amani, A., Kabiri, T., Shafiee, S., & Hamidi, A. (2019). Preparation and characterization of PLA-PEG-PLA/PEI/DNA nanoparticles for improvement of transfection efficiency and controlled release of DNA in gene delivery systems. *Iranian Journal of Pharmaceutical Research, 18*(1), 125–141.
13. Leopold, L. F., Tódor, I. S., Diaconeasa, Z., Rugină, D., Ştefancu, A., Leopold, N., & Coman, C. (2017). Assessment of PEG and BSA-PEG gold nanoparticles cellular interaction. *Colloids and Surfaces A: Physicochemical and Engineering Aspects, 532*(July), 70–76. https://doi.org/10.1016/j.colsurfa.2017.06.061.
14. Su, L., Shu, T., Wang, Z., Cheng, J., Xue, F., Li, C., & Zhang, X. (2013). Biosensors and bioelectronics immobilization of bovine serum albumin-protected gold nanoclusters by using polyelectrolytes of opposite charges for the development of the reusable fluorescent Cu^{2+}-sensor. *Biosensors and Bioelectronic, 44*, 16–20. https://doi.org/10.1016/j.bios.2013.01.005.
15. Conde, J., Ambrosone, A., Sanz, V., Hernandez, Y., Marchesano, V., Tian, F., Child, H., Berry, C. C., Ibarra, M. R., Baptista, P. V., Tortiglione, C., & de la Fuente, J. M. (2012). Design of multifunctional gold nanoparticles for in vitro and in vivo gene silencing. *ACS Nano, 6*(9), 8316–8324. https://doi.org/10.1021/nn3030223.
16. Paciotti, G. F., Kingston, D. G. I., & Tamarkin, L. (2006). *Colloidal gold nanoparticles: a novel nanoparticle platform for developing multifunctional tumor-targeted drug delivery vectors* (Vol. 54, pp. 47–54). https://doi.org/10.1002/ddr.
17. Sadzuka, Y., Kishi, K., Hirota, S., Sonobe, T. (2003). Effect of polyethyleneglycol (PEG) chain on cell uptake of PEG-modified liposomes, 13(2), 157–172. https://doi.org/10.1081/LPR-120020318.
18. Lipka, J., Semmler-behnke, M., Sperling, R. A., Wenk, A., Takenaka, S., Schleh, C., et al. (2010). Biomaterials biodistribution of PEG-modified gold nanoparticles following intratracheal instillation and intravenous injection. *Biomaterials, 31*(25), 6574–6581. https://doi.org/10.1016/j.biomaterials.2010.05.009.

19. Suk, J. S., Xu, Q., Kim, N., Hanes, J., & Ensign, L. M. (2016). PEGylation as a strategy for improving nanoparticle-based drug and gene delivery. *Advanced Drug Delivery Reviews, 99*(Pt A), 28–51. https://doi.org/10.1016/j.addr.2015.09.012.
20. Peter, John, H. J. T. Cooper. (1951). A study of the nucleation and growth process in the synthesis of colloidal gold. *Discussions of the Faraday Society*, 55(c), 55–75. https://doi.org/10.1039/df9511100055
21. Murdock, R. C., Braydich-Stolle, L., Schrand, A. M., Schlager, J. J., & Hussain, S. M. (2008). Characterization of nanomaterial dispersion in solution prior to in vitro exposure using dynamic light scattering technique. *Toxicological Sciences, 101*(2), 239–253. https://doi.org/10.1093/toxsci/kfm240.
22. Zhang, X. D., Wu, D., Shen, X., Liu, P. X., Yang, N., Zhao, B., et al. (2011). Size-dependent in vivo toxicity of PEG-coated gold nanoparticles. *International Journal of Nanomedicine, 6*, 2071–2081. https://doi.org/10.2147/IJN.S21657.
23. Bartczak, D., & Kanaras, A. G. (2011). Preparation of peptide-functionalized gold nanoparticles using one pot EDC/Sulfo-NHS coupling. *Langmuir, 27*(16), 10119–10123. https://doi.org/10.1021/la2022177.
24. Vijayakumar, S., & Ganesan, S. (2012). In vitro cytotoxicity assay on gold nanoparticles with different stabilizing agents. *Journal of Nanomaterials, 2012*, 1–9. https://doi.org/10.1155/2012/734398.
25. Steckiewicz, K. P., Barcinska, E., Malankowska, A., Zauszkiewicz–Pawlak, A., Nowaczyk, G., Zaleska-Medynska, A., & Inkielewicz-Stepniak, I. (2019). Impact of gold nanoparticles shape on their cytotoxicity against human osteoblast and osteosarcoma in in vitro model. Evaluation of the safety of use and anti-cancer potential. *Journal of Materials Science: Materials in Medicine, 30*(2), 1–15. https://doi.org/10.1007/s10856-019-6221-2.
26. Chen, C., Cheng, Y. C., Yu, C. H., Chan, S. W., Cheung, M. K., & Yu, P. H. F. (2008). In vitro cytotoxicity, hemolysis assay, and biodegradation behavior of biodegradable poly(3-hydroxybutyrate)-poly(ethylene glycol)-poly(3-hydroxybutyrate) nanoparticles as potential drug carriers. *Journal of Biomedical Materials Research - Part A, 87*(2), 290–298. https://doi.org/10.1002/jbm.a.31719.
27. Rahme, K., Chen, L., Hobbs, R. G., Morris, M. A., O'Driscoll, C., & Holmes, J. D. (2013). PEGylated gold nanoparticles: polymer quantification as a function of PEG lengths and nanoparticle dimensions. *RSC Advances, 3*(17), 6085–6094. https://doi.org/10.1039/c3ra22739a.
28. Moghimi, S. M., & Szebeni, J. (2003). Stealth liposomes and long circulating nanoparticles: critical issues in pharmacokinetics, opsonization and protein-binding properties, 42, 463–478. https://doi.org/10.1016/S0163-7827(03)00033-X
29. Urcan, E., Haertel, U., Styllou, M., Hickel, R., Scherthan, H., & Xaver, F. (2009). Real-time xCELLigence impedance analysis of the cytotoxicity of dental composite components on human gingival fibroblasts, 6, 51–58. https://doi.org/10.1016/j.dental.2009.08.007
30. Ju, P., Liang, R., Lee, Y., Zeng, Z., & Chuang, S. (2015). Differential cytotoxic effects of gold nanoparticles in different mammalian cell lines. *Journal of Hazardous Materials, 264*(2014), 303–312. https://doi.org/10.1016/j.jhazmat.2013.11.031.
31. Dobrovolskaia, M. A., Clogston, J. D., Neun, B. W., Hall, J. B., Patri, A. K., & McNeil, S. E. (2008). Method for analysis of nanoparticle hemolytic properties in vitro. *Nano Letters, 8*(8), 2180–2187. https://doi.org/10.1021/nl0805615.
32. Iwasaki, T., Ishibashi, J., Tanaka, H., Sato, M., Asaoka, A., Taylor, D. M., & Yamakawa, M. (2009). Selective cancer cell cytotoxicity of enantiomeric 9-mer peptides derived from beetle defensins depends on negatively charged phosphatidylserine on the cell surface. *Peptides, 30*(4), 660–668. https://doi.org/10.1016/j.peptides.2008.12.019.
33. Erdem, S. S., Obeidin, V. A., Yigitbasi, T., Tumer, S. S., & Yigit, P. (2018). Verteporfin mediated sequence dependent combination therapy against ovarian cancer cell line. *Journal of Photochemistry and Photobiology B: Biology, 183*(April), 266–274. https://doi.org/10.1016/j.jphotobiol.2018.04.039.
34. Öztaş, D. Y., Altunbek, M., Uzunoglu, D., Yllmaz, H., Cetin, D., Suludere, Z., & Culha, M. (2019). Tracing size and surface chemistry-dependent endosomal uptake of gold nanoparticles using surface-enhanced Raman scattering. *Langmuir, 35*(11), 4020–4028. https://doi.org/10.1021/acs.langmuir.8b03988.
35. Farooq, M. U., Novosad, V., Rozhkova, E. A., Wali, H., Fateh, A. A., Neogi, P. B., et al. (2018). Gold nanoparticles-enabled efficient dual delivery of anticancer therapeutics to HeLa cells. *Scientific Reports, 8*(1), 1–12. https://doi.org/10.1038/s41598-018-21331-y.
36. Albanese, A., & Chan, W. C. W. (2011). Effect of gold nanoparticle aggregation on cell uptake and toxicity, (7), 5478–5489.
37. Foroozandeh, P., & Aziz, A. A. (2018). Insight into cellular uptake and intracellular trafficking of nanoparticles. Nanoscale Research Letters, 13(1), 1–12.
38. Chow, E. K. H., & Ho, D. (2013). Cancer nanomedicine: from drug delivery to imaging. *Science Translational Medicine, 5*(216), 216), 1–216),12. https://doi.org/10.1126/scitranslmed.3005872.

Publisher's Note Springer Nature remains neutral with regard to jurisdictional claims in published maps and institutional affiliations.

Springer

Affiliations

Nihan Verimli [1,2] · Ayşegül Demiral [2,3] · Hülya Yılmaz [4] · Mustafa Çulha [4] · S. Sibel Erdem [1,2]

[1]   International School of Medicine, Medical Biochemistry, Istanbul Medipol University, 34810 Istanbul, Turkey

[2]   Regenerative and Restorative Medical Research Center (REMER), 34810 Istanbul, Turkey

[3]   School of Engineering and Natural Sciences, Biomedical Engineering, Istanbul Medipol University, 34810 Istanbul, Turkey

[4]   Faculty of Engineering, Department of Genetics and Bioengineering, Yeditepe University, 34755 Istanbul, Turkey